

latitudes, consistent with paleobotanical evidence (31–33) (fig. S7).

Our results for the mid-Cretaceous are broadly applicable throughout Earth history and demonstrate that variations in atmospheric mass, whether through changes in pO_2 or other constituents (i.e., pN_2), were an important factor in climate forcing on geological time scales that must be included in paleoclimate models. We also note the broad inverse correlation between some pO_2 records [e.g., (1, 9)] and global climate change during the Phanerozoic; we speculate that, to the extent that atmospheric pO_2 and pCO_2 have been linked through photosynthetic productivity and organic carbon burial, O_2 may have amplified CO_2 -driven climate change.

REFERENCES AND NOTES

1. R. A. Berner, *Geochim. Cosmochim. Acta* **70**, 5653–5664 (2006).
2. A. C. Scott, I. J. Glasspool, *Proc. Natl. Acad. Sci. U.S.A.* **103**, 10861–10865 (2006).
3. R. A. Berner, D. E. Canfield, *Am. J. Sci.* **289**, 333–361 (1989).
4. R. A. Berner, *Am. J. Sci.* **309**, 603–606 (2009).
5. R. S. Arvidson, F. T. Mackenzie, M. Guidry, *Am. J. Sci.* **306**, 135–190 (2006).
6. N. M. Bergman, T. M. Lenton, A. J. Watson, *Am. J. Sci.* **304**, 397–437 (2004).
7. P. G. Falkowski et al., *Science* **309**, 2202–2204 (2005).
8. I. J. Glasspool, A. C. Scott, *Nat. Geosci.* **3**, 627–630 (2010).
9. R. Tappert et al., *Geochim. Cosmochim. Acta* **121**, 240–262 (2013).
10. IPCC, *Climate Change 2013: The Physical Science Basis. Contribution of Working Group I to the Fifth Assessment Report of the Intergovernmental Panel on Climate Change* (Cambridge Univ. Press, New York, 2013).
11. K. E. Trenberth, J. T. Fasullo, J. Kiehl, *Bull. Am. Meteorol. Soc.* **90**, 311–323 (2009).
12. K. L. Bice et al., *Paleoceanography* **21**, PA2002 (2006).
13. O. Friedrich, R. D. Norris, J. Erbacher, *Geology* **40**, 107–110 (2012).
14. I. M. Held, B. J. Soden, *J. Clim.* **19**, 5686–5699 (2006).
15. G. A. Vecchi, B. J. Soden, *J. Clim.* **20**, 4316–4340 (2007).
16. M. R. Allen, W. J. Ingram, *Nature* **419**, 224–232 (2002).
17. D. L. Royer, *Geochim. Cosmochim. Acta* **70**, 5665–5675 (2006).
18. E. Barron, *Earth Sci. Rev.* **19**, 305–338 (1983).
19. C. J. Poulsen, *Nature* **432**, 814–815 (2004).
20. J. Zhou, C. J. Poulsen, N. Rosenbloom, C. Shields, B. Briegleb, *Clim. Past* **8**, 565–576 (2012).
21. M. Huber, R. Caballero, *Clim. Past* **7**, 603–633 (2011).
22. G. Ludvigson et al., *Geology* **26**, 1039 (1998).
23. H. Hasegawa et al., *Clim. Past* **8**, 1323–1337 (2012).
24. T. White, L. Gonzalez, G. Ludvigson, C. Poulsen, *Geology* **29**, 363 (2001).
25. A. H. Jähren, L. Sternberg, *Geology* **31**, 463–466 (2003).
26. A. Herman, R. Spicer, *Nature* **380**, 330–333 (1996).
27. D. R. Greenwood, J. F. Basinger, R. Y. Smith, *Geology* **38**, 15–18 (2010).
28. D. J. Peppe et al., *New Phytol.* **190**, 724–739 (2011).
29. P. A. Hayes, J. E. Francis, D. J. Cantrill, J. A. Crame, *Paleoclimate analysis of Late Cretaceous angiosperm leaf floras, James Ross Island, Antarctica. Geol. Soc. London Spec. Pub.* **258**, 49–62 (2006).
30. R. A. Spicer, A. B. Herman, *Paleogeogr. Palaeoclimatol. Palaeoecol.* **295**, 423–442 (2010).
31. R. Spicer, J. Parrish, *Geology* **14**, 703–706 (1986).
32. E. Peralta-Medina, H. J. Falcon-Lang, *Geology* **40**, 219–222 (2012).
33. J. E. Francis, I. Poole, *Paleogeogr. Palaeoclimatol. Palaeoecol.* **182**, 47–64 (2002).

ACKNOWLEDGMENTS

Supported by NSF Sedimentary Geology and Paleobiology Program grant F035175 and NSF Marine Geology and Geophysics grant F033663. We thank R. Feng, R. Fiorella, I. Montañez, and

three anonymous reviewers for discussion of and comments on this work. The model data are available at www.ncdc.noaa.gov/data-access/paleoclimatology-data/contributing.

SUPPLEMENTARY MATERIALS

www.sciencemag.org/content/348/6240/1238/suppl/DC1
Materials and Methods

Supplementary Text
Figs. S1 to S7
Tables S1 to S3
References (34–39)

2 September 2014; accepted 5 May 2015
10.1126/science.1260670

BRAIN NETWORKS

Correlated gene expression supports synchronous activity in brain networks

Jonas Richiardi,^{1,2,*} Andre Altmann,^{1,†} Anna-Clare Milazzo,^{3,1} Catie Chang,⁴ M. Mallar Chakravarty,^{5,6} Tobias Banaschewski,⁷ Gareth J. Barker,⁸ Arun L.W. Bokde,⁹ Uli Bromberg,¹⁰ Christian Büchel,¹⁰ Patricia Conrod,^{8,11} Mira Fauth-Bühler,¹² Herta Flor,¹³ Vincent Frouin,¹⁴ Jürgen Gallinat,¹⁵ Hugh Garavan,^{9,16} Penny Gowland,¹⁷ Andreas Heinz,¹⁵ Hervé Lemaître,^{18,19} Karl F. Mann,¹² Jean-Luc Martinot,^{18,19} Frauke Nees,¹³ Tomáš Paus,^{20,21} Zdenka Pausova,²² Marcella Rietschel,²³ Trevor W. Robbins,²⁴ Michael N. Smolka,²⁵ Rainer Spanagel,²⁶ Andreas Ströhle,¹⁵ Gunter Schumann,^{8,27} Mike Hawrylycz,²⁸ Jean-Baptiste Poline,²⁹ Michael D. Greicius,^{1,*} IMAGEN consortium[‡]

During rest, brain activity is synchronized between different regions widely distributed throughout the brain, forming functional networks. However, the molecular mechanisms supporting functional connectivity remain undefined. We show that functional brain networks defined with resting-state functional magnetic resonance imaging can be recapitulated by using measures of correlated gene expression in a post mortem brain tissue data set. The set of 136 genes we identify is significantly enriched for ion channels. Polymorphisms in this set of genes significantly affect resting-state functional connectivity in a large sample of healthy adolescents. Expression levels of these genes are also significantly associated with axonal connectivity in the mouse. The results provide convergent, multimodal evidence that resting-state functional networks correlate with the orchestrated activity of dozens of genes linked to ion channel activity and synaptic function.

Brain activity at rest exhibits intrinsic low-frequency synchronization between anatomically distinct brain regions (1). When observed with functional magnetic resonance imaging (fMRI), this coherence between regions (functional connectivity) defines 15 to 20 brain networks associated with such canonical functions as vision, language, episodic memory, and spatial attention (2–4). These functional networks are disrupted in several neurodegenerative and neuropsychiatric diseases (5) and may constitute the maps followed by neurodegenerative diseases marching, trans-synaptically, across the brain (6). Although it has been shown that connectivity within the default-mode network (DMN) (7) and topological measures of whole-brain networks (8) are heritable, the set of genes promoting functional connectivity remains unknown. To pursue this question, we applied a network modeling approach to both neuroimaging and gene expression data.

Using resting-state fMRI data from 15 healthy right-handed subjects (eight females, age range 18 to 29 years), we computed 14 well-known and

reproducible functional networks (fig. S1) (9) by using independent component analysis (ICA). We then mapped samples from the Allen Institute for Brain Science (AIBS) human microarray data set (six subjects, two contributed both hemispheres, four contributed one hemisphere, one female, age range 24 to 57 years, totaling 3702 brain samples) (table S1) (10) to these networks by using normalized Montreal Neurological Institute (MNI) coordinates. To avoid biases due to gross transcriptional dissimilarities in different brain regions, we excluded basal ganglia, cerebellum, and deep gray matter (including hippocampus), leaving only cortex samples (data file S1). This removed the basal ganglia network, leaving 13 networks. Of 1777 cortex samples, 501 were mapped to the 13 functional networks, and 1276 to “non-network” regions of the brain. We focused the analysis on four large nonoverlapping networks: dorsal default-mode (dDMN), salience, sensorimotor, and visuospatial (Fig. 1A), comprising 241 samples total. These four networks were chosen because they are well characterized in the imaging literature (2, 11–14),

consist of noncontiguous regions in both hemispheres, and have adequate coverage in the AIBS data (Fig. 1B).

We used the transcriptional similarity of gene expression profiles between brain tissue samples to define correlated gene expression networks. In mouse brains, transcriptional similarity reflects cytoarchitecture (15), but in human brains, the differences are more subtle across the neocortex (10). As opposed to gene coexpression networks, which quantify gene-gene relationships across tissue samples (16), a correlated gene expression network quantifies tissue-tissue relationships across genes. Nodes were defined by brain tissue samples (Fig. 1B); edges were weighted

by similarity between vectors of gene expression values at each sample. After preprocessing and assigning one probe for each of the 16,906 genes (data file S2) (17), we measured expression similarity by means of Pearson correlation (17), setting negative correlations to zero. Then we asked whether there are observable genetic correlates for the functional network organization: Are gene expression correlations in functionally grouped regions higher than can be expected by chance?

We defined the strength fraction in functional networks as a measure of the relationship between correlated gene expression within and outside the set of functional networks of interest. Denoting W the sum of all edge weights within all functional networks, W_i the sum of weights within the four functional networks of interest, and T the brain graph's total strength (sum of all edge weights linking the full 1777-nodes graph), the strength fraction is $S = W_i / (T - W)$. Higher values of S mean that the samples in the set of functional networks are more similar to each other, relative to the remaining brain regions (fig. S2). We assessed significance using permutation testing (18), randomly reshuffling 10,000 times the sample-to-network assignment in the full 1777-nodes graph. In addition to considering only cortex samples, so as to avoid biasing results toward similar tissues (10), before computation we removed edges linking two samples belonging to the same tissue class [defined by means of regional ontology (fig. S3 and table S4)]. Grouping gene expression samples according to functional networks yielded a higher strength fraction than that of other groupings of samples; the spatial organization of functional networks corresponded to regions that have more highly correlated gene expression than expected by chance ($P < 10^{-4}$). Given that we used only cortical samples, that we removed edges linking tissues of the same class, and that functional networks are spatially distributed, this finding cannot emerge from spatial proximity or gross tissue similarity.

We next sought to identify which genes, specifically, drive the relationship between correlated gene expression and functional networks. We computed the marginal influence of each gene on strength fraction of all four functional networks together (17) and ranked genes across all six different two-way splits of the six subjects (17). Then, we computed list overlap statistics (19) between the two brain subgroups at a false discovery rate (FDR) of 5%. Combining results from six splits, the final list was obtained via stability selection (20), selecting genes that appear in the majority of splits (four or more out of six). This resulted in a consensus list of 136 genes (table S2).

We validated our findings in vivo (supplementary text) using paired genome-wide single-nucleotide polymorphism (SNP) data and resting state fMRI (rs-fMRI) recordings in $n = 259$ 14-year-olds (126 females) from the IMAGEN database (21), which has more subjects, but not all were usable (data file S3) (17). The strength fraction

for the combined four networks in the rs-fMRI data was computed for every subject (as in the AIBS gene expression data) and used as a quantitative imaging phenotype in a genome-wide association study (GWAS) (fig. S4), correcting for several covariates, including motion. We computed a z statistic (22) for the enrichment of P values in the consensus list. Genetic variation in the consensus list was significantly associated with in vivo rs-fMRI strength fraction ($z = 2.55$, $P = 0.006$). Thus, not only gene expression levels but also common polymorphisms in the consensus genes were related to the strength of functional networks. Subjects at both ends of the spectrum of multilocus genetic scores [representing the multiallelic effect of the genes in the consensus list on the functional connectivity phenotype (17)] showed definite differences in functional connectivity strength mostly within the functional networks themselves, but also between the functional networks (Fig. 2 and fig. S5).

We next investigated the relationship between our gene list and the connectivity of axonal projections underlying functional networks. We used the Allen Institute mouse brain atlas (15), which offers finely sampled whole-genome expression data, together with a recent mesoscale model of mouse connectivity derived from the Allen Mouse Brain Connectivity Atlas (AMBCA) (23). To match human data, we focused on the mouse isocortex and used a 38-region parcellation (Fig. 3A) (23). With 57 mouse orthologs for our consensus gene list, we obtained a correlated gene expression network, representing transcriptional similarity between these 38 regions. We computed a normalized, symmetric connectivity matrix from the significant connections in the ipsilateral connectivity model of the AMBCA (17). We tested the association between the mouse connectivity graph and transcriptional similarity graph (Fig. 3, B and C) using a modified Mantel procedure; we randomly selected gene subsets of the same size as our ortholog consensus list 10,000 times in order to obtain a null distribution. The correlation between transcriptional similarity in these 38 mesoscale isocortex regions and their axonal connectivity was significantly higher when using our list than expected by chance ($P = 0.011$, or $P = 0.022$ when using the contralateral connectivity model).

Last, we categorized the consensus gene list using Gene Ontology (GO) by computing statistical overrepresentation for Biological Processes (BP), Cellular Component (CC), and Molecular Function (MF) with the Database for Annotation, Visualization, and Integrated Discovery (DAVID) 6.7 (24). The only significant MF annotation [$P < 0.05$, Benjamini-Hochberg False Discovery Rate (FDR_{BH})-corrected] related to ion transport. No BP annotation was significant. Four out of six significant CC annotations ($P < 0.03$ FDR_{BH}) concerned ion channels, in particular involving sodium channels such as SCN4B or receptors such as GABRA5 (full annotation list is available in tables S5 and S6). Significant associations with nine diseases, including Alzheimer's disease and schizophrenia

¹Functional Imaging in Neuropsychiatric Disorders

Laboratory, Department of Neurology and Neurological Sciences, Stanford University, Stanford, CA, USA.

²Laboratory of Neurology and Imaging of Cognition,

Department of Neuroscience, University of Geneva, Geneva, Switzerland.

³The War Related Illness and Injury Study Center, VA Palo Alto Health Care System, Palo Alto, CA, USA.

⁴Advanced MRI Section, Laboratory of Functional and Molecular Imaging, National Institute of Neurological Disorders and Stroke, National Institutes of Health, Bethesda, MD, USA.

⁵Cerebral Imaging Centre, Douglas Mental Health University Institute, Montreal, Canada.

⁶Departments of Psychiatry and Biomedical Engineering, McGill University, Montreal, Canada.

⁷Department of Child and Adolescent Psychiatry, Central Institute of Mental Health, Medical Faculty Mannheim, Heidelberg University, Mannheim, Germany.

⁸Institute of Psychiatry, Psychology and Neuroscience, King's College London, London, UK.

⁹Institute of Neuroscience, Trinity College Dublin, Dublin, Ireland.

¹⁰Universitätsklinikum Hamburg Eppendorf, Hamburg, Germany.

¹¹Department of Psychiatry, Université de Montréal, Centre Hospitalier Universitaire (CHU) Ste Justine Hospital, Montréal, Canada.

¹²Department of Addictive Behaviour and Addiction Medicine, Central Institute of Mental Health, Medical Faculty Mannheim, Heidelberg University, Mannheim, Germany.

¹³Department of Cognitive and Clinical Neuroscience, Central Institute of Mental Health, Medical Faculty Mannheim, Heidelberg University, Mannheim, Germany.

¹⁴Neurospin, Commissariat à l'Energie Atomique et aux Energies Alternatives, Paris, France.

¹⁵Department of Psychiatry and Psychotherapy, Campus Charité Mitte, Charité-Universitätsmedizin Berlin, Berlin, Germany.

¹⁶Departments of Psychiatry and Psychology, University of Vermont, Burlington, VT, USA.

¹⁷School of Physics and Astronomy, University of Nottingham, Nottingham, UK.

¹⁸Institut National de la Santé et de la Recherche Médicale, INSERM Unit 1000 "Neuroimaging and Psychiatry,"

University Paris Sud, Orsay, France.

¹⁹INSERM Unit 1000 at Maison de Solenn, Assistance Publique Hôpitaux de Paris (APHP), Cochin Hospital, University Paris Descartes, Sorbonne Paris Cité, Paris, France.

²⁰Rotman Research Institute, University of Toronto, Toronto, Canada.

²¹School of Psychology, University of Nottingham, Nottingham, UK.

²²The Hospital for Sick Children, University of Toronto, Toronto, Canada.

²³Department of Genetic Epidemiology in Psychiatry, Central Institute of Mental Health, Medical Faculty Mannheim, Heidelberg University, Mannheim, Germany.

²⁴Behavioural and Clinical Neuroscience Institute and Department of Psychology, University of Cambridge, Cambridge, UK.

²⁵Department of Psychiatry and Psychotherapy, and Neuroimaging Center, Technische Universität Dresden, Dresden, Germany.

²⁶Department of Psychopharmacology, Central Institute of Mental Health, Faculty of Clinical Medicine Mannheim, Mannheim, Germany.

²⁷Medical Research Council (MRC) Social, Genetic and Developmental Psychiatry (SGDP) Centre, London, UK.

²⁸Allen Institute for Brain Science, Seattle, WA, USA.

²⁹Helen Wills Neuroscience Institute, University of California Berkeley, Berkeley, CA, USA.

*Corresponding author. E-mail: jonas.richiardi@unige.ch (J.R.); greicius@stanford.edu (M.D.G.)

†These authors contributed equally to this work. ‡IMAGEN consortium (www.imagen-europe.com) authors and affiliations are listed in the supplementary materials.

§These authors contributed equally to this work. ¶IMAGEN consortium (www.imagen-europe.com) authors and affiliations are listed in the supplementary materials.

‡These authors contributed equally to this work. ‡IMAGEN consortium (www.imagen-europe.com) authors and affiliations are listed in the supplementary materials.

‡These authors contributed equally to this work. ‡IMAGEN consortium (www.imagen-europe.com) authors and affiliations are listed in the supplementary materials.

‡These authors contributed equally to this work. ‡IMAGEN consortium (www.imagen-europe.com) authors and affiliations are listed in the supplementary materials.

‡These authors contributed equally to this work. ‡IMAGEN consortium (www.imagen-europe.com) authors and affiliations are listed in the supplementary materials.

‡These authors contributed equally to this work. ‡IMAGEN consortium (www.imagen-europe.com) authors and affiliations are listed in the supplementary materials.

‡These authors contributed equally to this work. ‡IMAGEN consortium (www.imagen-europe.com) authors and affiliations are listed in the supplementary materials.

‡These authors contributed equally to this work. ‡IMAGEN consortium (www.imagen-europe.com) authors and affiliations are listed in the supplementary materials.

‡These authors contributed equally to this work. ‡IMAGEN consortium (www.imagen-europe.com) authors and affiliations are listed in the supplementary materials.

‡These authors contributed equally to this work. ‡IMAGEN consortium (www.imagen-europe.com) authors and affiliations are listed in the supplementary materials.

‡These authors contributed equally to this work. ‡IMAGEN consortium (www.imagen-europe.com) authors and affiliations are listed in the supplementary materials.

‡These authors contributed equally to this work. ‡IMAGEN consortium (www.imagen-europe.com) authors and affiliations are listed in the supplementary materials.

‡These authors contributed equally to this work. ‡IMAGEN consortium (www.imagen-europe.com) authors and affiliations are listed in the supplementary materials.

‡These authors contributed equally to this work. ‡IMAGEN consortium (www.imagen-europe.com) authors and affiliations are listed in the supplementary materials.

‡These authors contributed equally to this work. ‡IMAGEN consortium (www.imagen-europe.com) authors and affiliations are listed in the supplementary materials.

‡These authors contributed equally to this work. ‡IMAGEN consortium (www.imagen-europe.com) authors and affiliations are listed in the supplementary materials.

‡These authors contributed equally to this work. ‡IMAGEN consortium (www.imagen-europe.com) authors and affiliations are listed in the supplementary materials.

‡These authors contributed equally to this work. ‡IMAGEN consortium (www.imagen-europe.com) authors and affiliations are listed in the supplementary materials.

‡These authors contributed equally to this work. ‡IMAGEN consortium (www.imagen-europe.com) authors and affiliations are listed in the supplementary materials.

‡These authors contributed equally to this work. ‡IMAGEN consortium (www.imagen-europe.com) authors and affiliations are listed in the supplementary materials.

‡These authors contributed equally to this work. ‡IMAGEN consortium (www.imagen-europe.com) authors and affiliations are listed in the supplementary materials.

‡These authors contributed equally to this work. ‡IMAGEN consortium (www.imagen-europe.com) authors and affiliations are listed in the supplementary materials.

‡These authors contributed equally to this work. ‡IMAGEN consortium (www.imagen-europe.com) authors and affiliations are listed in the supplementary materials.

‡These authors contributed equally to this work. ‡IMAGEN consortium (www.imagen-europe.com) authors and affiliations are listed in the supplementary materials.

‡These authors contributed equally to this work. ‡IMAGEN consortium (www.imagen-europe.com) authors and affiliations are listed in the supplementary materials.

‡These authors contributed equally to this work. ‡IMAGEN consortium (www.imagen-europe.com) authors and affiliations are listed in the supplementary materials.

‡These authors contributed equally to this work. ‡IMAGEN consortium (www.imagen-europe.com) authors and affiliations are listed in the supplementary materials.

‡These authors contributed equally to this work. ‡IMAGEN consortium (www.imagen-europe.com) authors and affiliations are listed in the supplementary materials.

‡These authors contributed equally to this work. ‡IMAGEN consortium (www.imagen-europe.com) authors and affiliations are listed in the supplementary materials.

‡These authors contributed equally to this work. ‡IMAGEN consortium (www.imagen-europe.com) authors and affiliations are listed in the supplementary materials.

‡These authors contributed equally to this work. ‡IMAGEN consortium (www.imagen-europe.com) authors and affiliations are listed in the supplementary materials.

‡These authors contributed equally to this work. ‡IMAGEN consortium (www.imagen-europe.com) authors and affiliations are listed in the supplementary materials.

($P < 0.05$ FDR_{BH}), which are network disorders, were also found (table S10). We validated annotations in vivo on IMAGEN data by restricting the analysis to these seven significant GO terms. Genetic variation in all but 1 GO term was significantly associated with in vivo functional connectivity ($z > 4.02$, $P < 2.8 \times 10^{-5}$ uncorrected) (table S9). Using a mouse transcriptome database (25), we also found that 39 mouse orthologs from our list were significantly enriched in neurons, 19 in astrocytes, and 14 in oligodendrocytes (76 were not significantly over-expressed in any of these three cell types). This

suggests that the relationship between gene expression and spatial organization into functional networks may be due to neuronal processes more than to support cell or white-matter processes.

Functional networks are fundamental to many brain processes in humans. Here, we show that network strength was correlated with the expression of genes tightly linked to synaptic function. The preservation of the association between functional networks and gene expression across the lifespan (IMAGEN, 14-year-olds; AIBS, 24- to 55-year-olds) is remarkable and could be partly explained by the relative stabilization of inter-

regional transcriptional similarity from adolescence onwards (26). Genes in our list may also play a role in certain diseases; some are implicated in brain disorders such as Alzheimer's and schizophrenia (27), whose pathogenesis is thought to relate, in part, to aberrant connectivity. Beyond humans, it appears that similar mechanisms extend to lower animals because our list is significantly associated with mouse neural connectivity, and several gene functions from our list were found in a study examining genes supporting neural connectivity in rodents (tables S3, S7, and S8) (28). Thus, our results show that across

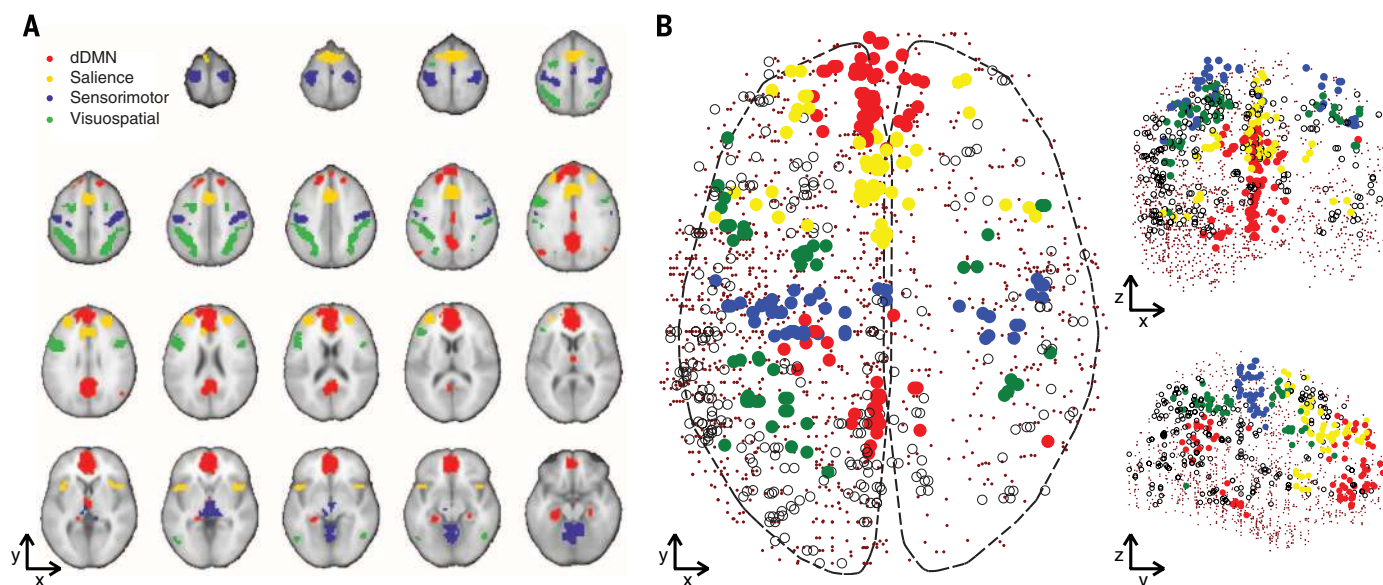


Fig. 1. Functional networks in MRI and gene expression data. (A) The four functional networks of interest. Red, dorsal default mode; yellow, salience; green, visuospatial; blue, sensorimotor. (B) AIBS brain samples assigned to their corresponding functional network. Solid circles are samples assigned to the four networks of interest, open circles show samples in the nine other networks, and dots show non-network AIBS samples.

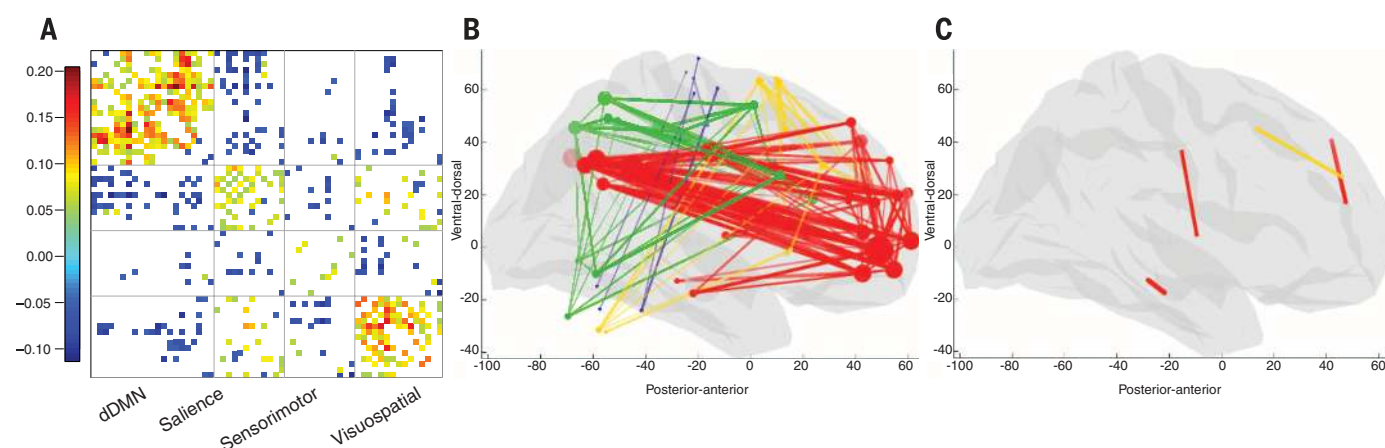


Fig. 2. In vivo functional connectivity differences related to the consensus gene list. Difference in in vivo functional connectivity between the averages of the top 20 and the bottom 20 subjects in IMAGEN, ranked by genotype score with respect to the consensus list of genes. (A) Difference matrix sorted by functional network (correlation differences smaller than $|0.05|$ are not shown). Positive values indicate connections that are stronger in high genotype score subjects, and negative values indicate the opposite. Connections are mostly increased within functional networks, but also be-

tween some functional networks. (B) MNI space sagittal view of within-network connections that are stronger in high-genotype-score subjects. Regions (disks) are coded according to the functional network they belong to: red, dorsal default mode; yellow, salience; green, visuospatial; blue, sensorimotor. Connections (lines) are color-coded to their functional networks. (C) Same, for connections that are stronger in low-genotype-score subjects. The majority of connections are strengthened in high-genotype-score subjects.

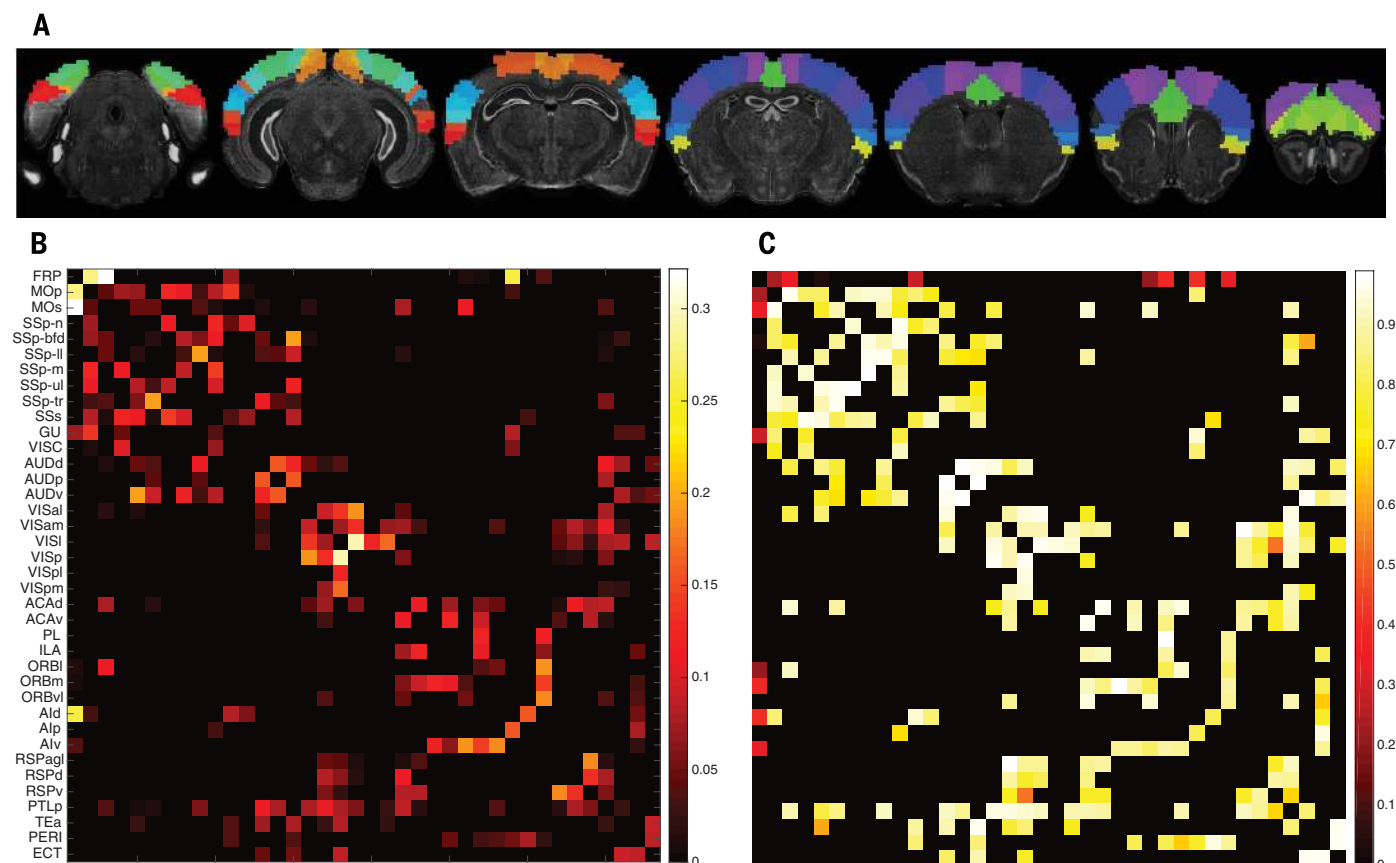


Fig. 3. Mouse mesoscale connectivity and transcriptional similarity. (A) Mouse isocortex parcellated into 38 regions (23). (B) Corresponding symmetrized, thresholded, and normalized ipsilateral axonal connectivity weights. (C) Transcriptional similarity (genetic correlation), using our consensus list of genes.

developmental stages and species, functional connectivity in brain networks is integrally linked to the machinery of synaptic communication.

REFERENCES AND NOTES

- M. D. Fox, M. E. Raichle, *Nat. Rev. Neurosci.* **8**, 700–711 (2007).
- S. M. Smith *et al.*, *Proc. Natl. Acad. Sci. U.S.A.* **106**, 13040–13045 (2009).
- R. M. Birn, *Neuroimage* **62**, 864–870 (2012).
- Z. Shehzad *et al.*, *Cereb. Cortex* **19**, 2209–2229 (2009).
- M. D. Fox, M. Greicius, *Front. Syst. Neurosci.* **4**, 19 (2010).
- W. W. Seeley, R. K. Crawford, J. Zhou, B. L. Miller, M. D. Greicius, *Neuron* **62**, 42–52 (2009).
- D. C. Glahn *et al.*, *Proc. Natl. Acad. Sci. U.S.A.* **107**, 1223–1228 (2010).
- A. Fornito *et al.*, *J. Neurosci.* **31**, 3261–3270 (2011).
- W. R. Shirer, S. Ryali, E. Rykhlevskaia, V. Menon, M. D. Greicius, *Cereb. Cortex* **22**, 158–165 (2012).
- M. J. Hawrylycz *et al.*, *Nature* **489**, 391–399 (2012).
- D. Mantini, M. G. Perrucci, C. Del Gratta, G. L. Romani, M. Corbetta, *Proc. Natl. Acad. Sci. U.S.A.* **104**, 13170–13175 (2007).
- N. U. F. Dosenbach *et al.*, *Proc. Natl. Acad. Sci. U.S.A.* **104**, 11073–11078 (2007).
- Y. Golland, P. Golland, S. Bentin, R. Malach, *Neuropsychologia* **46**, 540–553 (2008).
- S. D. Roosendaal *et al.*, *Brain* **133**, 1612–1621 (2010).
- L. Ng *et al.*, *Nat. Neurosci.* **12**, 356–362 (2009).
- B. Zhang, S. Horvath, *Stat. Appl. Genet. Mol. Biol.* **4**, e17 (2005).
- Materials and methods are available as supplementary materials on Science Online.
- J. Richiardi, A. Altman, M. Greicius, in *Proceedings of the 3rd International Workshop on Pattern Recognition in Neuroimaging (PRNI)* (PRNI, Philadelphia, 2013), pp. 70–73.
- L. Natarajan, M. Pu, K. Messer, *Ann. Appl. Stat.* **6**, 521–541 (2012).
- N. Meinshausen, P. Bühlmann, *J. R. Stat. Soc. Series B Stat. Methodol.* **72**, 417–473 (2010).
- G. Schumann *et al.*, IMAGEN consortium, *Mol. Psychiatry* **15**, 1128–1139 (2010).
- D. Nam, J. Kim, S.-Y. Kim, S. Kim, *Nucleic Acids Res.* **38** (Web Server), W749–W754 (2010).
- S. W. Oh *et al.*, *Nature* **508**, 207–214 (2014).
- W. Huang, B. T. Sherman, R. A. Lempicki, *Nat. Protoc.* **4**, 44–57 (2009).
- J. D. Cahoy *et al.*, *J. Neurosci.* **28**, 264–278 (2008).
- M. Pletikos *et al.*, *Neuron* **81**, 321–332 (2014).
- A. Heck *et al.*, *Neuron* **81**, 1203–1213 (2014).
- L. Wolf, C. Goldberg, N. Manor, R. Sharan, E. Ruppin, *PLOS Comput. Biol.* **7**, e1002040 (2011).
- normal brain function and psychopathology) (LSHM-CT- 2007-037286), the FP7 projects IMAGEMEND (602450; IMAGING GENetics for MENTAL Disorders) and MATRICS (603016), the Innovative Medicine Initiative Project EU-AIMS (115300-2), a Medical Research Council Programme Grant “Developmental pathways into adolescent substance abuse” (93558), the Swedish funding agency FORMAS, the Medical Research Council and the Wellcome Trust (Behavioral and Clinical Neuroscience Institute, University of Cambridge), the National Institute for Health Research (NIHR) Biomedical Research Centre at South London and Maudsley NHS Foundation Trust and King’s College London, the Bundesministerium für Bildung und Forschung (BMBF; grants 01GS08152, 01EV0711, eMED SysAlc01ZX1311A, and Forschungsnetz AERIAL), the Deutsche Forschungsgemeinschaft (DFG; grants FOR 1617, EXC 257, SM 80/7-1, SM 80/7-2, and SFB 940/1), the U.S. National Institutes of Health (Axon, Testosterone and Mental Health during Adolescence; RO1 MH085772-01A1), Eranet-Neuron grant (project AF12-NEUR0008-01 - WM2NA), MILDECA, Fondation pour la Recherche Médicale, NIH Consortium grant U54 EB020403, which is supported by a cross-NIH alliance that funds Big Data to Knowledge Centers of Excellence, and the Allen Institute for Brain Science.

ACKNOWLEDGMENTS

We thank C.-K. Lee for help with AIBS data normalization and C. Quairiaux for help with mouse brain anatomy. Functional networks imaging data are at http://findlab.stanford.edu/functional_ROIs.html. Human microarray data are at <http://human.brain-map.org>. IMAGEN data are available by application to consortium coordinator G. Schumann (<http://imagen-europe.com>) after evaluation according to an established procedure. Mouse gene expression data are at <http://mouse.brain-map.org>. Connectivity model data are from (23). J.R. is supported by a Marie Curie Fellowship from the European Union (299500). M.D.G. is supported by grants from the Feldman Family Foundation and the National Institutes of Health (RO1NS073498). This work received additional support from the following sources: the European Union-funded FP6 Integrated Project IMAGEN (Reinforcement-related behavior in

SUPPLEMENTARY MATERIALS

www.sciencemag.org/content/348/6240/1241/suppl/DC1
Materials and Methods
Supplementary Text
Figs. S1 to S5
Tables S1 to S10
IMAGEN Consortium Author List
References (29–55)
Data Files S1 to S3

12 May 2014; accepted 7 May 2015
10.1126/science.1255905